Supporting information

Coupled effects of Mn(Ⅱ), pH and anionic ligands on the reactivity of nanostructured birnessite

Qinzhi Li[a], Rasesh Pokharel[a], Lian Zhou[a], Mathieu Pasturel[b], Khalil Hanna[a,c] *

[a]*Univ. Rennes, École Nationale Supérieure de Chimie de Rennes, CNRS, ISCR – UMR6226, F-35000 Rennes, France*
[b] *Univ. Rennes, CNRS, ISCR – UMR 6226, F-35000, Rennes, France*
[c]*Institut Universitaire de France (IUF), MESRI, 1 rue Descartes, 75231 Paris, France.*

*Corresponding author: Tel.: +33 2 23 23 80 27, khalil.hanna@ensc-rennes.fr (K. Hanna)

17 Figures, 18 pages

ATR-FTIR. ATR-FTIR (Golden Gate, single bounce diamond, Specab) data were collected with a IS50 Nicolet FTIR spectrometer equipped with a DLaTGS detector at room temperature. Centrifuged wet pastes were placed in the ATR cell. All spectra of wet pastes were collected by subtracting spectral contributions of supernatant as a background from the raw materials. Measurements were carried out over the range of 600−4000 cm^{-1} at a spectral resolution of 4.0 cm^{-1} with the forward/reverse scanning rate of 10 Hz and 1000 coadded spectra scans for each sample.

Detection of byproducts by chromatographic analysis. The PIP_{ox} were analyzed by a Waters ultra HPLC-MS (Acquity UPLC) using a Waters BEH C18 column (100 mm×2.1 mm, 1.7 μm). The mobile phase consisted of acetonitrile containing 0.1% of formic acid (eluant A) and mixture acetonitrile/water 10%/90% containing 0.1% of formic acid (eluant B) with gradient 0 min/0% A – 1 min/0% A – 9 min/100% A – 12 min/0% A, and a flow rate of 400 μL/min. An electrospray interface (ESI) was used for the MS measurements in positive ionization mode and full scan acquisition.

Oxalic acid-permanganate back-titration method. 0.1 g of the acid birnessite was dissolved in 2.5 mL of 0.5 M $H_2C_2O_4$ and 5 mL of 1 M H_2SO_4 to reduce all highly charged manganese ions to Mn(Ⅱ). After all samples to be dissolved, the excess $C_2O_4^{2-}$ was back titrated with standardized 0.02 M $KMnO_4$ solution at 75–85℃ until the color of solution turned into reddish and lasted for 30 seconds without fading, to obtain the oxidation number of Mn. Then, 0.1 g of the acid birnessite sample was dissolved in 20 mL 0.25 M hydroxylamine hydrochloride and diluted to 2 L with ultrapure water. AAS was used to determine the total Mn content, and the Mn content of the synthesized acid birnessite is 51.42 (±2.6) wt%. Then, according to the titration result and total Mn content, the AOS of acid birnessite was calculated. Triplicates were performed for each sample and the mean AOS value can be calculated.

$$AOS=2+54.94 * \frac{n(\ the\ oxidation\ number, mol\ )}{m(\ the\ total\ Mn\ content, g)}$$

A chain reaction of PIP oxidation by MnO_2

Step 1: Formation of precursor complex

$>Mn^{IV} + PIP \rightarrow (>Mn^{IV}, PIP)$

Step 2: Electron transfer within the precursor complex generating $>Mn^{III}$ and PIP_{ox}

$>Mn^{IV} + PIP \rightarrow (>Mn^{III}, PIP_{ox})$

Step 3: Further reaction of $>Mn^{III}$ with available PIP to generate stable Mn^{II} and PIP_{ox}

$(>Mn^{III} + PIP) \rightarrow Mn^{II} + PIP_{ox}$

Step 4: PIP_{ox} could further oxidize to form additional byproducts

$PIP_{ox} \rightarrow$ secondary byproducts

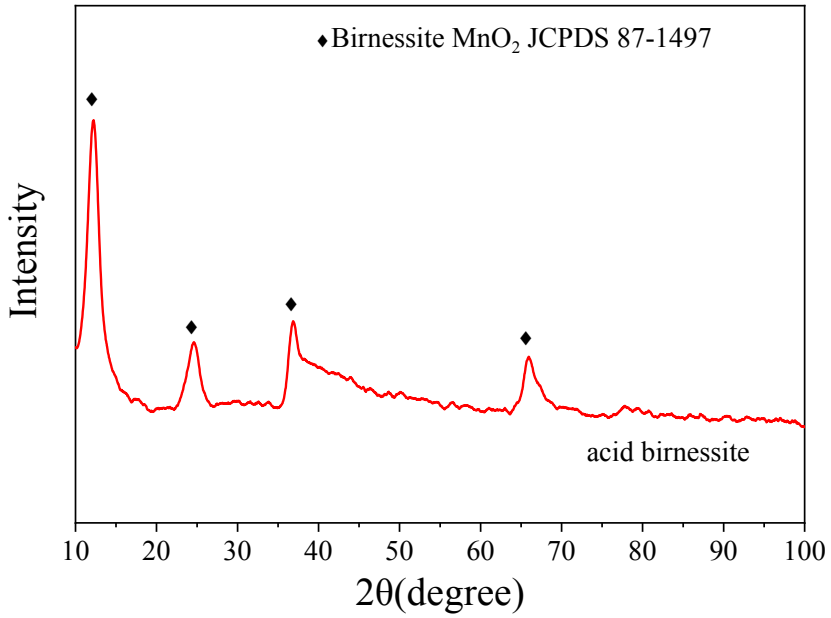

Figure S1. XRD pattern of acid birnessite.

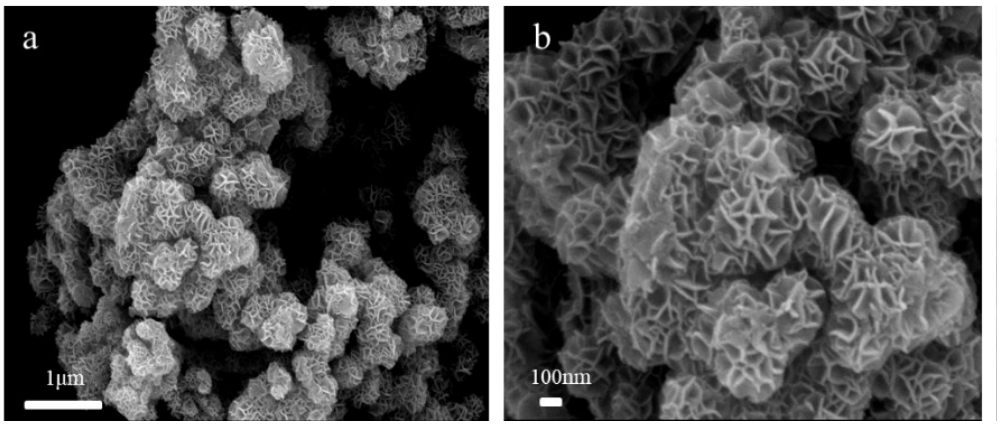

Figure S2. SEM images of synthesized acid birnessite, exhibiting the shape of nanoflower spheres with a ~300nm diameter size.

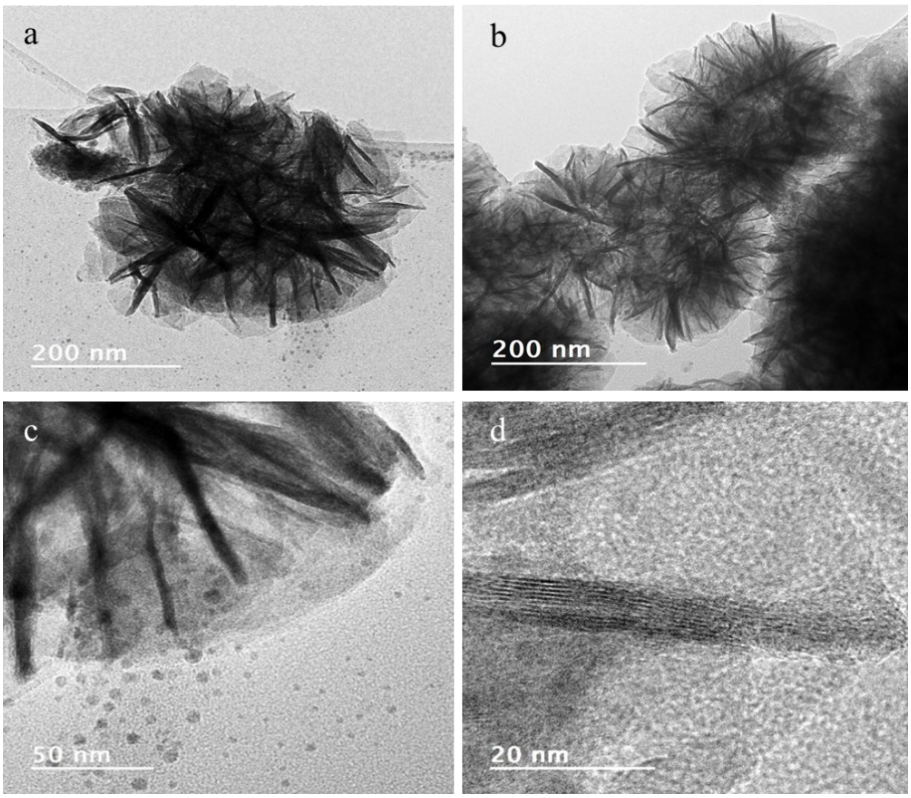

Figure S3. TEM images showing how nanoflakes agglomerate to form aggregates and then small flower-like nanoparticles or nanopetals.

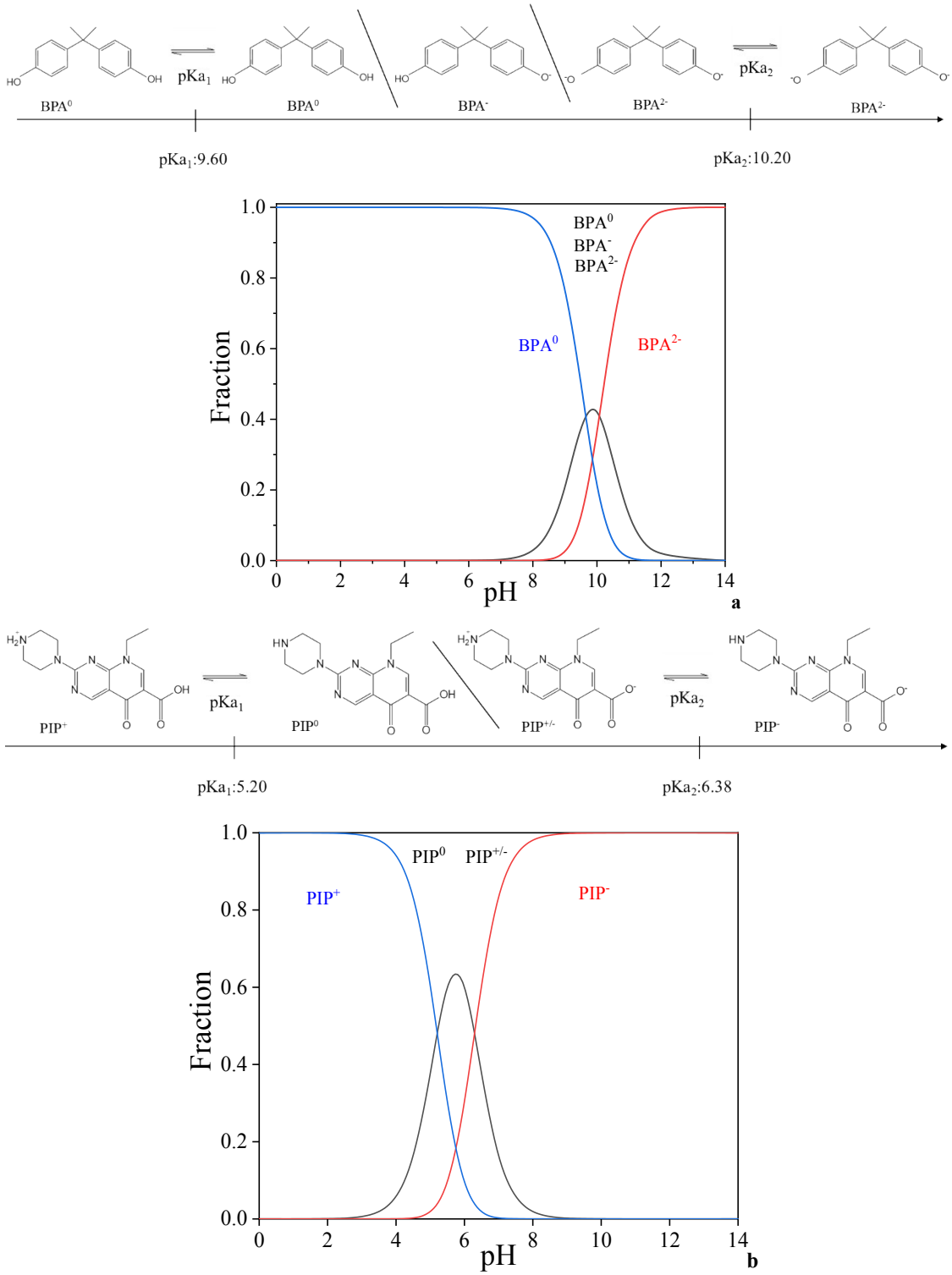

Figure S4. Chemical speciation of BPA(a) and PIP(b) *vs* pH. Ionic strength: 10 mM NaCl. pK_{as} of BPA ($pK_{a,1}$ =9.60 and $pK_{a,2}$ =10.20) and PIP ($pK_{a,1}$ =5.20 and $pK_{a,2}$ =6.38) at infinite dilution were obtained from conditional pK_a values and the Davies equation.

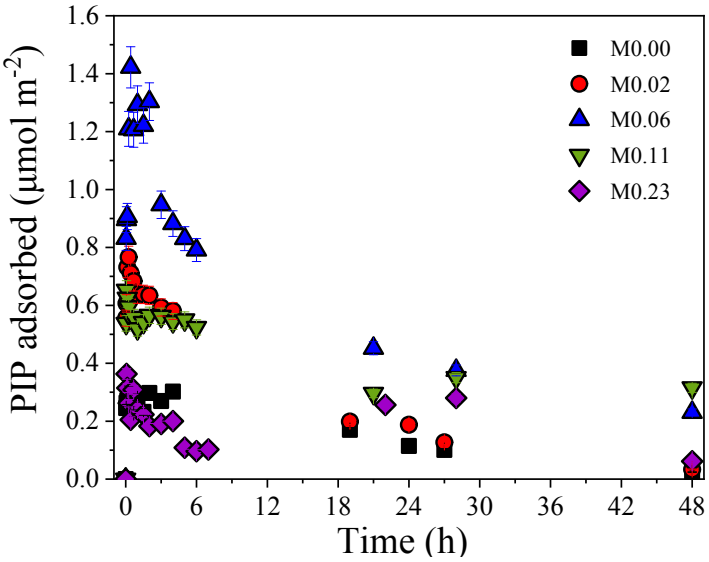

Figure S5. PIP adsorption data plotted as a function of time at different Mn(Ⅱ)/MnO_2 ratio. Experimental conditions: $[PIP]_0$ =20 μM; [acid birnessite]$_0$ =870 μM; $[NaCl]_0$ =10 mM; pH =5.5 ±0.1.

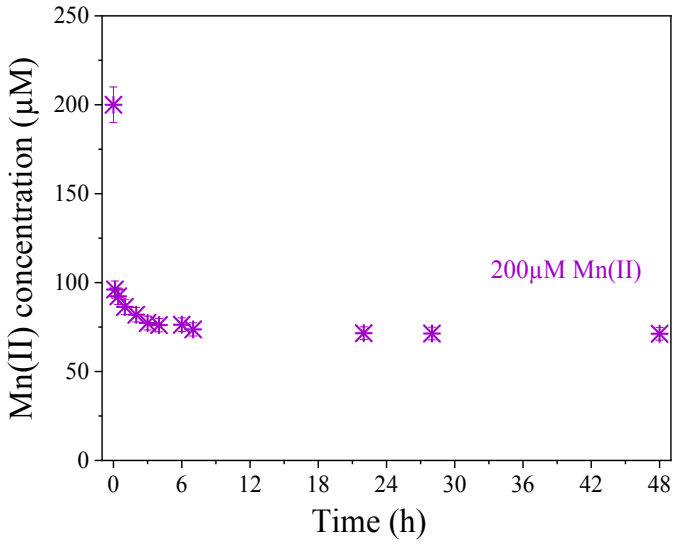

Figure S6. Mn(II) concentration in the suspension versus reaction time in the presence of 200 μM Mn(II) at pH 5.5 ±0.1. Experimental conditions: $[PIP]_0$ =20 μM; [acid birnessite]$_0$ =870 μM; $[Mn(II)]_0$ =200 μM; $[NaCl]_0$ =10 mM.

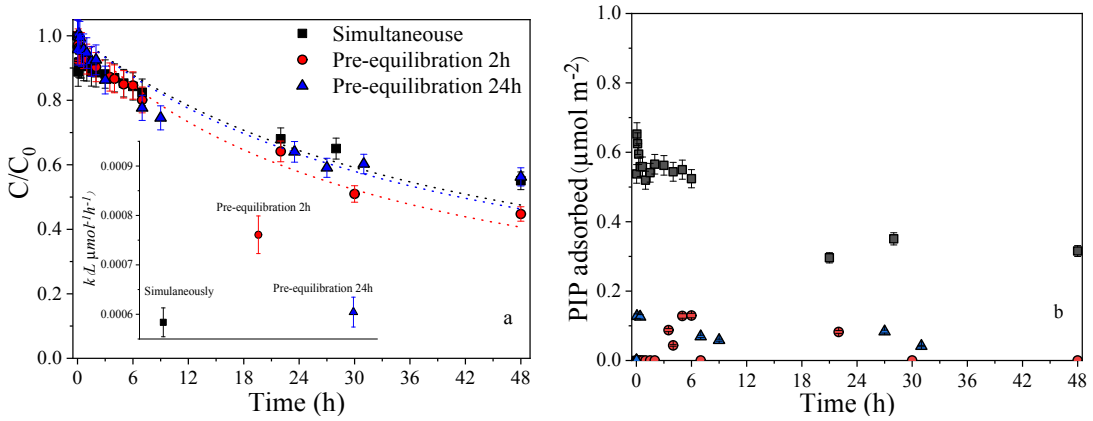

Figure S7. Removal kinetics and kinetic rate constants (inset) of PIP(a), PIP adsorption data plotted as a function of timec(b) at different pre-equilibration time (0, 2 and 24 h) in the presence of 100 μM Mn(II) at pH 5.5 ±0.1. Dotted lines represent the pseudo-second-order kinetic model (a). Pre-equilibration experiments imply a mixture of solution of 100 μM Mn(II) and 870 μM acid birnessite for 2 h or 24 h before PIP addition. Experimental conditions: $[PIP]_0$ =20 μM; $[\text{acid birnessite}]_0$ =870 μM; $[NaCl]_0$ =10 mM; $[Mn(II)]_0$ =100 μM.

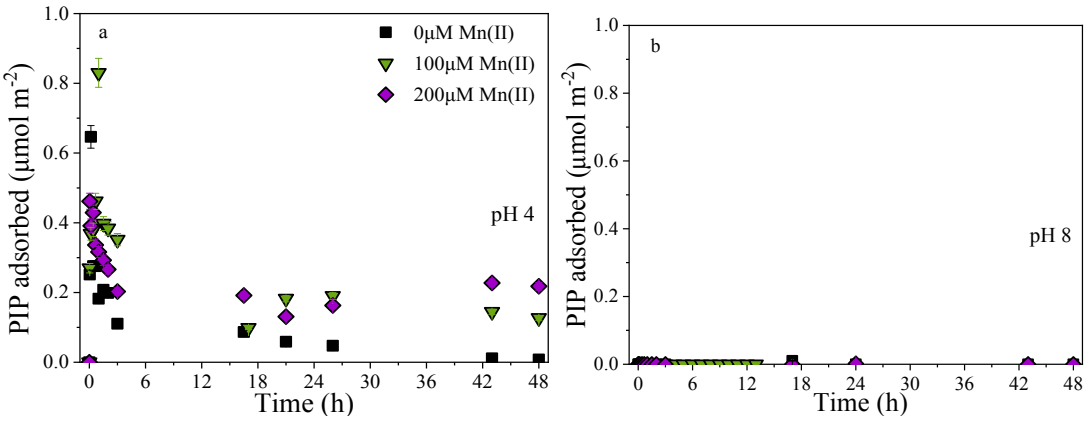

Figure S8. PIP adsorption data plotted as a function of time at different initial Mn(II) concentration and pH 4 ±0.1(a), pH 8 ±0.1(b). Experimental conditions: $[PIP]_0$ =20 μM; $[\text{acid birnessite}]_0$ =870 μM; $[NaCl]_0$ =10 mM; $[Mn(II)]_0$ =0, 100, 200 μM.

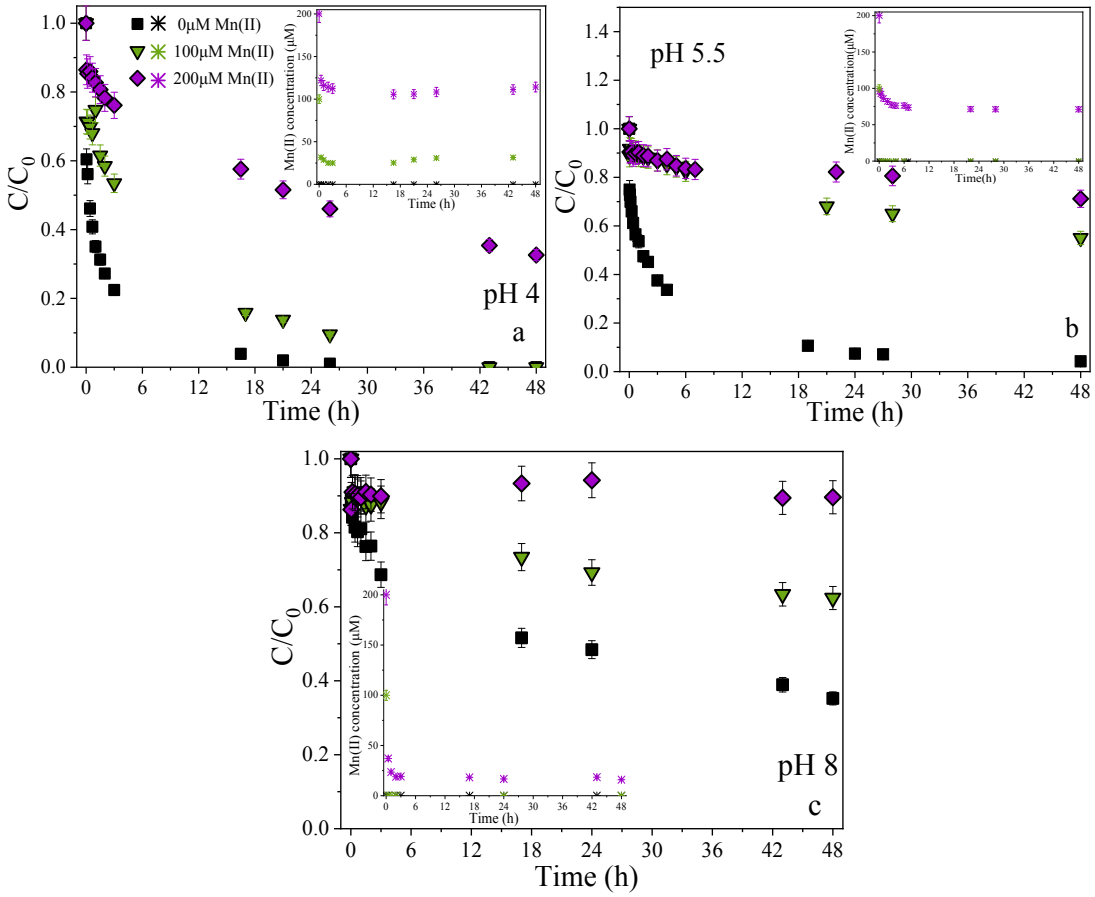

Figure S9. Removal kinetics of PIP (total concentration after desorption) and dissolved Mn(Ⅱ) (inset) at different initial concentrations of Mn(Ⅱ) (0, 100, 200 μM) and pH 4 ±0.1(a), 5.5 ±0.1(b), 8 ±0.1(c). Experimental conditions: $[PIP]_0$ =20 μM; [acid birnessite]$_0$ = 870 μM; $[NaCl]_0$ =10 mM.

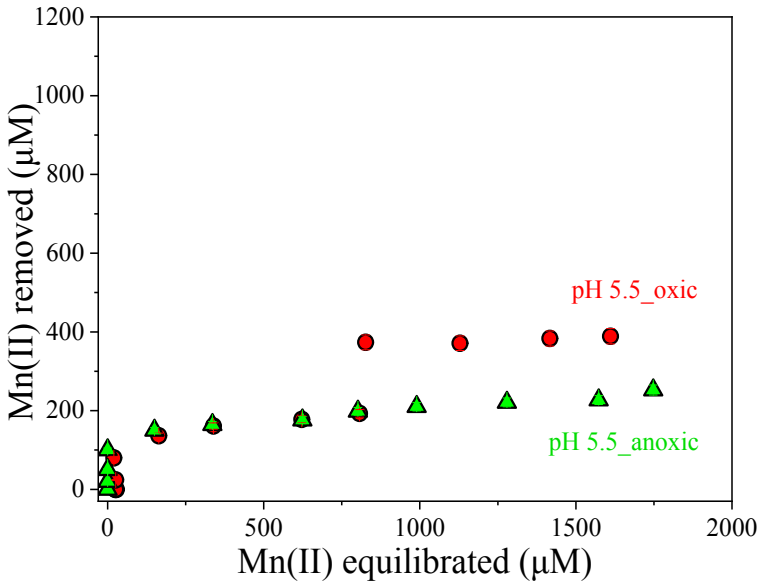

Figure S10. Comparison of oxic and anoxic Mn(II)-birnessite sorption isotherms at pH 5.5 ±0.1. Experimental conditions: $[\text{acid birnessite}]_0$ =870 μM; $[\text{NaCl}]_0$ =10 mM; reaction time =2 d.

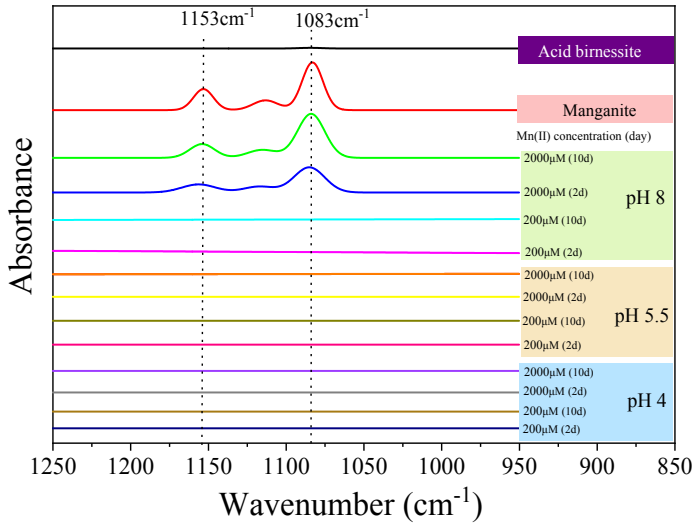

Figure S11. ATR-FTIR spectra of as-prepared Mn-oxides (Acid birnessite, Manganite) and Mn(II)-birnessite sorption samples reacted under oxic conditions at different Mn(II) concentration (200 μM, 2000 μM) and pH 4, 5.5, 8 ±0.1 for 2 d or 10 d. The black vertical dotted lines represent OH bending modes allowing identification of manganite (1153, 1083 cm^{-1}). Experimental conditions: $[\text{acid birnessite}]_0$ =870 μM; $[NaCl]_0$ =10 mM.

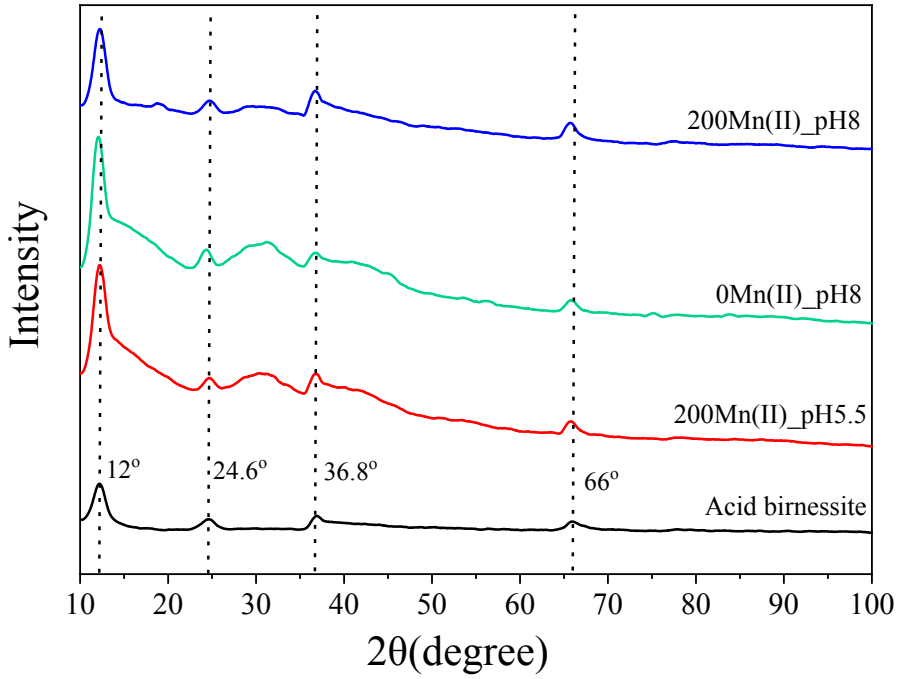

Figure S12. XRD patterns of as-prepared acid birnessite (Acid birnessite) and kinetic samples collected after reaction of PIP and acid birnessite in the presence of Mn(Ⅱ) (48 h). 200Mn(Ⅱ)_pH8, 0Mn(Ⅱ)_pH8, 200Mn(Ⅱ)_pH5.5 indicate the initial supplied Mn(Ⅱ) concentration of 200 μM, 0 μM and 200 μM during the redox reactions at pH 8, 8, 5.5 ±0.1, respectively. The vertical dotted lines indicate the peaks of acid birnessite (12˚, 24.6˚, 36.8˚, 66˚). Experimental conditions: $[PIP]_0$ =20 μM; $[\text{acid birnessite}]_0$ =870 μM; $[NaCl]_0$ =10 mM.

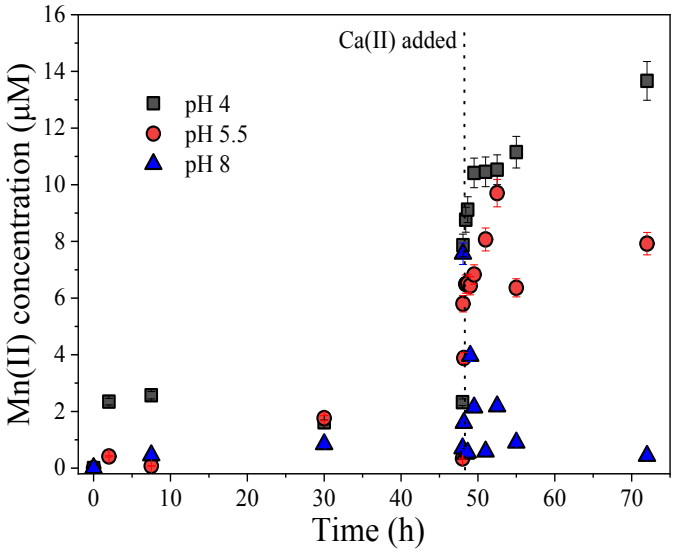

Figure S13. Mn(Ⅱ) concentration in the suspension desorbed by Ca(Ⅱ) after PIP oxidation by acid birnessite (48 h) at pH 4, 5.5, 8 ±0.1. The black vertical dotted lines indicate the time of Ca(Ⅱ) added (48 h). Experimental conditions: $[PIP]_0$ =20 μM; [acid birnessite]$_0$ =870 μM; $[NaCl]_0$ =10 mM; $[CaCl_2]_0$ =25 mM.

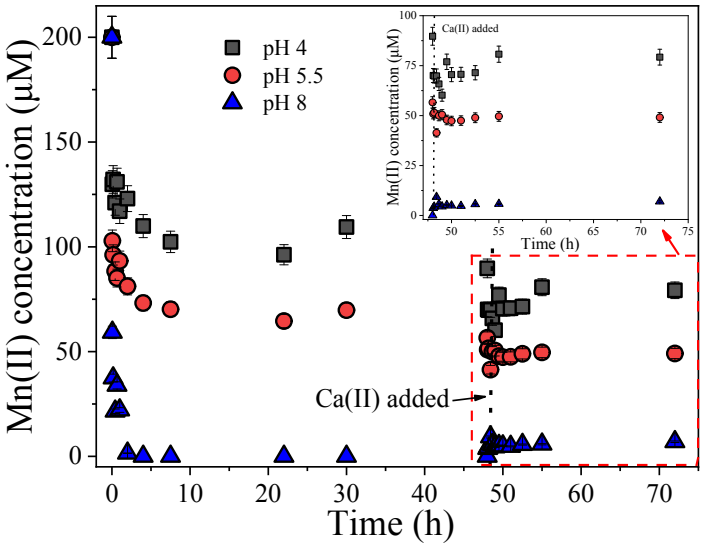

Figure S14. Mn(Ⅱ) concentration in the suspension desorbed by Ca(Ⅱ) after PIP oxidation by acid birnessite (48 h) in the presence of 200 μM Mn(Ⅱ) at pH 4, 5.5, 8 ±0.1. The black vertical dotted lines indicate the time of Ca(Ⅱ) added (48 h).

Experimental conditions: $[Mn(II)]_0$ =200 μM; [acid birnessite]$_0$ =870 μM; $[NaCl]_0$ =10 mM; $[CaCl_2]_0$ =25 mM.

Two-site sorption model approach

The adsorption and oxidation reaction of PIP at the acid birnessite surface under the combined effect of Mn(II), pH and inorganic ligands was simulated using a two-site reversible batch sorption kinetics model based on mass conservation law for solute from batch reaction tests. [1,2] The mass balance equation for aqueous mass in the batch system could be described as:

$$VC + m_s S = VC_{in} \quad (1)$$

where C, C_{in} is the aqueous concentration at time t (h) and initial respectively (μmol/L), V is solution volume (L), m_s is mass of adsorbent (kg), S is the sorbed concentration (μmol/kg). The two-site model is based on the assumption that aqueous phase concentration decreases continuously as a result of instantaneous and kinetic sorption reaction at the edge site. Thus, S is the sum of sorbed concentration in Type 1 reversible equilibrium sorption (S_1, equilibrium sorption to "instantaneous" sites that can be assimilated to oxidation) and Type 2 nonequilibrium or kinetic sorption (S_2, nonequilibrium sorption to "kinetic" sites).

$$\frac{\partial S_1}{\partial t} = fK_d \frac{\partial C}{\partial t} \quad (2)$$

$$\frac{\partial S_2}{\partial t} = \alpha\left[(1-f)K_d C - S_2\right] \quad (3)$$

where S_1 and S_2 are sorbed-phase concentrations of PIP on the instantaneous and kinetic sorption sites at time t (μmol/kg), respectively, f is the fraction of Type-1 sorption site, α is the rate constant for mass transfer from aqueous phase to sorption site (h^{-1}), and K_d is the distribution coefficient (L/kg). Since PIP oxidation is a surface-controlled process, adsorption onto surface sites (S_2) could be considered as the rate-limiting step in the whole removal process.

Then, the relationship between the liquid concentration ($C^*=C/C_{in}$) versus time (t) can be obtained as follows [3]:

$$\frac{\partial C^*}{\partial t} = -\frac{\alpha}{\beta}\left[C^* - \frac{1}{R}\right] \quad (4)$$

where $R = 1 + \frac{m_s K_d}{V}$, with R as the retardation factor, $\beta = \frac{V + m_s f K_d}{V + m_s K_d}$, with β as a limiting factor for S_2 and its range $0 < \beta \leqslant 1$.

$$C^* = \frac{1}{R} + (1-\beta)\, e^{-\frac{\alpha}{\beta}t}$$

Based on this model, three parameters such as sorption rate constant α, Type-1 faction f, distribution or partitioning coefficient K_d can be estimated by fitting sorption kinetic data using nonlinear curve on the C/C_{in} *vs* time. Thus, a series of experiments are normalized to one line by plotting C/C_{in} *vs* time (Table S1 and Figure S16). Both K_d and α decreased with increasing in Mn(Ⅱ) concentration over the pH investigated range, suggesting that Mn(II) can alter both adsorption and oxidation.

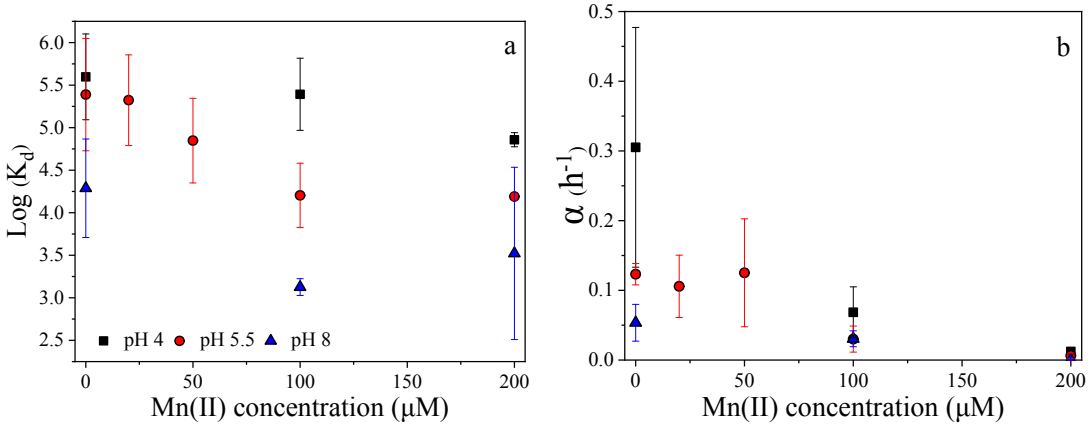

Figure S15. Modeling parameters (K_d, α) of PIP *vs* Mn(Ⅱ) concentration for kinetic experiments at pH 4, 5.5, 8 ±0.1. Experimental conditions: $[PIP]_0$ =20 μM; [acid birnessite]$_0$ =870 μM; $[NaCl]_0$ =10 mM.

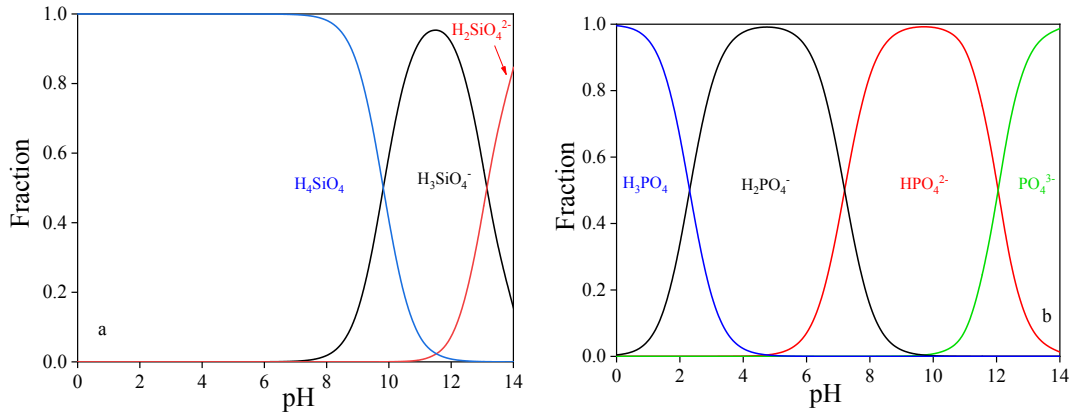

Figure S16. Chemical speciation of (a) silicate (Na_2SiO_3) and (b) phosphate(NaH_2PO_4) versus pH. pK_{as} of silicate ($pK_{a,1}$ =9.82 and $pK_{a,2}$ =13.45) and phosphate ($pK_{a,1}$ =2.12, $pK_{a,2}$ =7.21 and $pK_{a,3}$ =12.31) at infinite dilution were obtained from conditional pK_a values and the Davies equation.

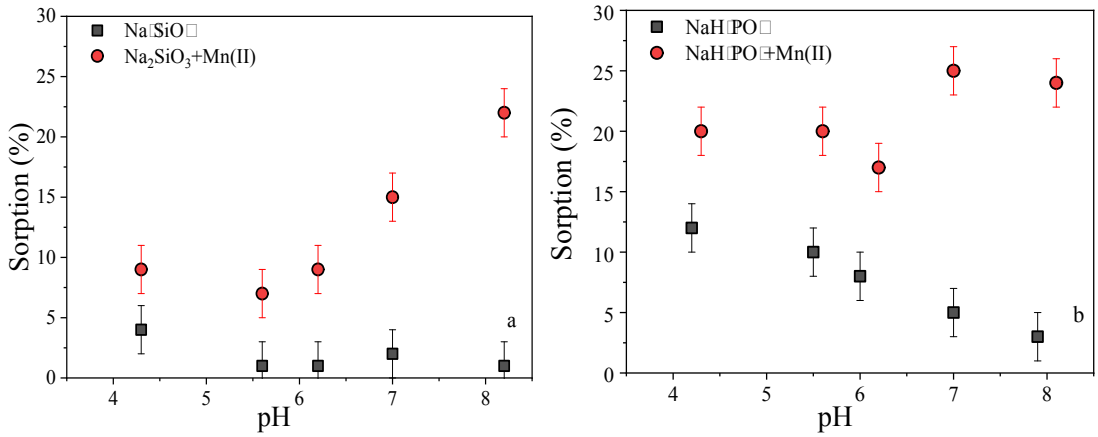

Figure S17. Sorption of (a) silicate (Na_2SiO_3) and (b) phosphate(NaH_2PO_4) with acid birnessite as a function of pH in presence/absence of dissolved Mn(Ⅱ). Experimental conditions: [acid birnessite]$_0$ =870 μM; [NaCl]$_0$ =10 mM; [Mn(Ⅱ)]$_0$ =100 μM; [Na_2SiO_3]$_0$ =100 μM; [NaH_2PO_4]$_0$ =100 μM; reaction time =48 h.

References

1 S. J. Lee, S. G. Chung, D. J. Kim, C. E. Lee and J. W. Choi, New method for determination of equilibrium/kinetic sorption parameters, *Curr. Appl. Phys*, 2009, **9,** 1323-1325.

2 P. Nkedi-Kizza, D. Shinde, M. R. Savabi, Y. Ouyang and L. Nieves, Sorption kinetics and equilibria of organic pesticides in carbonatic soils from South Florida, *J. Environ. Qual,* 2006, **35,** 268-276.

3 S. J. Lee, D. J. Kim and J. W. Choi, Comparison of first-order sorption kinetics using concept of two-site sorption model, *Environ. Sci. Technol*, 2012, **29,** 1002-1007.